Inorganic Chemistry

Article

pubs.acs.org/IC

A Combined Experimental and Theoretical Investigation on the Role of Halide Ligands on the Catecholase-like Activity of Mononuclear Nickel(II) Complexes with a Phenol-Based Tridentate Ligand

Jaydeep Adhikary,[†] Prateeti Chakraborty,[†] Sudhanshu Das,[†] Tanmay Chattopadhyay,[‡] Antonio Bauzá,[§] Shyamal Kumar Chattopadhyay,[⊥] Bipinbihari Ghosh,[⊥] Franz A. Mautner,*[,∥] Antonio Frontera,*[,§] and Debasis Das*[,†]

[†]Department of Chemistry, University of Calcutta, 92 A.P.C. Road, Kolkata 700 009, India

[‡]Department of Chemistry, Panchakot Mahavidyalaya, Sarbari, Purulia, Pin 723121, India

[§]Departament de Química, Universitat de les Illes Balears, Crta. de Valldemossa km 7.5, 07122 Palma (Baleares), Spain

[⊥]Department of Chemistry, Bengal Engineering and Science University, Howrah 711 103, India

[∥]Institut fuer Physikalische und Theoretische Chemie, Technische Universitaet Graz, 8010 Graz, Austria

Supporting Information

ABSTRACT: Three new mononuclear nickel(II) complexes, namely, $[NiL^1(H_2O)_3]I_2{\cdot}H_2O$ (**1**), $[NiL^1(H_2O)_3]Br_2{\cdot}H_2O$ (**2**), and $[NiL^1(H_2O)_3]Cl_2{\cdot}2H_2O$ (**3**) [HL^1 = 2-[(2-piperazin-1-ylethylimino)methyl]phenol], have been synthesized and structurally characterized. Structural characterization reveals that they possess similar structure: $[NiL^1(H_2O)_3]^{2+}$ complex cations, two halide counteranions, and lattice water molecules. One of the nitrogen atoms of the piperazine moiety is protonated to provide electrical neutrality to the system, a consequence observed in earlier studies (*Inorg. Chem.* **2010**, *49*, 3121; *Polyhedron* **2013**, *52*, 669). Catecholase-like activity has been investigated in methanol by a UV−vis spectrophotometric study using 3,5-di-*tert*-butylcatechol (3,5-DTBC) as the model substrate. Complexes **1** and **2** are highly active, but surprisingly **3** is totally inactive. The coordination chemistries of **1** and **2** remain unchanged in solution, whereas **3** behaves as a 1:1 electrolyte, as is evident from the conductivity study. Because of coordination of the chloride ligand to the metal in solution, it is proposed that 3,5-DTBC is not able to effectively approach an electrically neutral metal, and consequently complex **3** in solution does not show catecholase-like activity. Density functional theory (DFT) calculations corroborate well with the experimental observations and thus, in turn, support the proposed hypothesis of inactivity of **3**. The cyclic voltametric study as well as DFT calculations suggests the possibility of a ligand-centered reduction at −1.1 V vs Ag/AgCl electrode. An electron paramagnetic resonance (EPR) experiment unambiguously hints at the generation of a radical from EPR-inactive **1** and **2** in the presence of 3,5-DTBC. Generation of H_2O_2 during catalysis has also been confirmed. DFT calculations support the ligand-centered radical generation, and thus a radical mechanism has been proposed for the catecholase-like activity exhibited by **1** and **2**. Upon heating, **2** and **3** lose water molecules in two steps (first lattice waters, followed by coordinating water molecules), whereas **3** loses four water molecules in a single step, as revealed from thermogravimetric analysis. The totally dehydrated species are red, in all cases having square-planar geometry, and have amorphous nature, as is evident from a variable-temperature powder X-ray diffraction study.

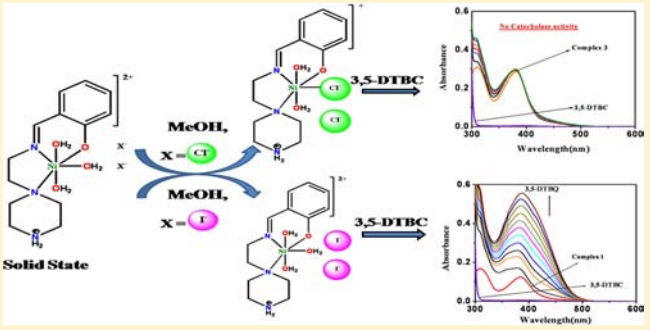

1. INTRODUCTION

Nickel(II) has very rich coordination chemistry owing to its inherent ability to adopt various geometries that are often interconvertible, and it is very well documented that such configurational or conformational changes are generally associated with color changes.[1−6] Interestingly, how a change in the coordination chemistry of nickel(II) may influence their catalytic property has not yet been properly addressed in the literature. Our group is continuously engaged in studying Schiff-base complexes of transition- and post-transition-metal ions, mainly as small synthetic analogues of metallobiosites like catechol oxidase, phosphatase, and cyt P-450 and as possible mimics of nucleases.[7−15] During our study to develop synthetic analogues of catechol oxidase, we synthesized a small dinuclear nickel(II) complex of 2,6-bis(*N*-ethylpiperazinyliminomethyl)-4-methylphenolate, and to our surprise, we observed an extraordinary catalytic activity of the complex to oxidize not

Received: July 15, 2013
Published: November 18, 2013

   dx.doi.org/10.1021/ic401819t | *Inorg. Chem.* 2013, 52, 13442−13452

only 3,5-di-*tert*-butylcatechol (3,5-DTBC) but also tetrachlorocatechol, a substrate that is very difficult to oxidize.[8] Critical analysis revealed that the extra positive charge on the ligand backbone might be instrumental for such extraordinary activity. That unprecedented finding inspired us to study the catalytic property of analogous mononuclear nickel(II) complexes. In that study again we noticed that complexes with ligand having extra positive charge (e.g., 2-[(2-piperazin-1-ylethylimino)-methyl]phenol; HL^1) after complexation exhibited catalytic activity in oxidizing 3,5-DTBC.[15] Incidentally, in all those cases, the counteranion was nitrate. So, we were not in a position to explore the role of the counteranion in manipulating the coordination chemistry of nickel(II) species and, consequently, their catalytic efficiency, particularly to catalyze the aerobic oxidation of 3,5-DTBC. In order to get faithful answers to all of those queries, as our first attempt, we synthesized (Scheme 1)

Scheme 1. Synthetic Route of Complexes 1−3

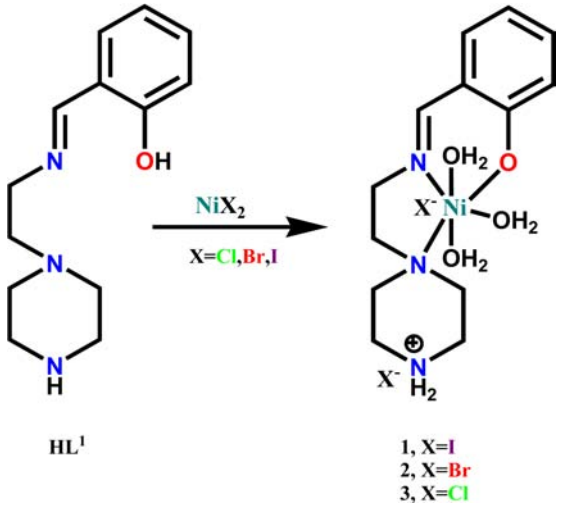

mononuclear nickel halide complexes, namely, $[NiL^1(H_2O)_3]I_2\cdot H_2O$ (**1**), $[NiL^1(H_2O)_3]Br_2\cdot H_2O$ (**2**), and $[NiL^1(H_2O)_3]Cl_2\cdot 2H_2O$ (**3**). All three complexes have been structurally characterized. Comprehensive investigations of their solid-state thermal properties, coordination behavior in solution, and catalytic activity to oxidize 3,5-DTBC have been performed to find out whether counteranions also have some role in influencing the catalytic activity of the complex. In spite of the very similar structural features of all three complexes in the solid state, complex **3** shows amazingly different coordination behavior in solution. Surprisingly, complex **3** shows inactivity in catalyzing aerobic oxidation of 3,5-DTBC, whereas the other two exhibit excellent catecholase-like activity. A conductance study followed by detailed density functional theory (DFT) calculations has been carried out to rationalize the unprecedented observation. Cyclic voltammetric (CV), differential pulse voltammetric (DPV), and electron paramagnetic resonance (EPR) studies have been performed to find out the origin of the catecholase-like activity exhibited by **1** and **2**, and DFT calculations further have been done to propose the possible mechanistic pathway involved in that activity.

2. EXPERIMENTAL SECTION

Physical Methods and Materials. Elemental analyses (carbon, hydrogen, and nitrogen) were performed using a Perkin-Elmer 240C elemental analyzer. IR spectra (4000−500 cm^{-1}) were recorded at 27 °C using a Perkin-Elmer RXI FT-IR spectrophotometer with KBr pellets. Electronic spectra (1400−200 nm) were obtained at 27 °C using a Shimadzu UV-3101PC spectrometer with methanol as the solvent and reference. Thermal analyses (TG−DTA) were carried out on a Mettler Toledo (TGA/SDTA851) thermal analyzer in flowing dinitrogen (flow rate: 30 cm^3 min^1). Ambient-temperature magnetic susceptibility measurements were performed with Magway MSB Mk1 magnetic susceptibility balance. Conductance of the methanolic solution of complexes was measured using a SYSTRONICS 306 conductivity meter. EPR experiments were performed at liquid-nitrogen temperature (77 K) in methanol, using a JEOL JES-FA200 spectrometer at X band (9.13 GHz). Cyclic and differential pulse voltammograms were recorded in MeCN solutions containing 0.1 M TEAP as the supporting electrolyte, using a CH1120A potentiostat with glassy carbon as the working electrode, platinum wire as the counter electrode, and Ag/AgCl/saturated KCl as the reference electrode. The ferrocene/ferrocenium couple was observed at E° (ΔE_p) = 0.48 V (100 mV) under our experimental conditions. Powder X-ray diffraction (PXRD) was performed on a XPERT-PRO diffractometer with monochromated Cu Kα radiation (40.0 kV and 30.0 mA) at room temperature. Nickel was estimated gravimetrically with dimethylglyoxime. All chemicals were obtained from commercial sources and used as received. Solvents were dried according to standard procedure and distilled prior to use. Salicylaldehyde, *N*-(2-aminoethyl)piperazine, nickel(II) chloride hexahydrate, nickel(II) bromide hydrate, nickel(II) iodide, and 3,5-di-*tert*-butylcatechol (3,5-DTBC) were purchased from Aldrich.

Synthesis of Complex $[NiL^1(H_2O)_3]I_2\cdot H_2O$ (1). A methanolic solution (5 mL) of *N*-(2-aminoethyl)pipeazine (0.258 g, 2 mmol) was added dropwise to a hot methanolic solution (10 mL) of salicylaldehyde (0.244g, 2 mmol), and the resulting solution was refluxed for 0.5 h. Then, a methanolic solution (5 mL) of NiI_2 (0.625g, 2 mmol) was added, and the resulting solution was stirred for 3−4 h. The green solution was filtered and kept in a $CaCl_2$ desiccator in the dark, and after a few days, crystals of complex **1**, suitable for X-ray data analysis, were obtained. Yield: 73%. Anal. Calcd for $C_{13}H_{27}N_3O_5I_2Ni$: C, 25.27; H, 4.4; N, 6.8; Ni, 9.46. Found: C, 25.21; H, 4.49; N, 6.72; Ni, 9.42. UV−vis−near-IR (methanol, nm): λ_{max} = 381, 629, 753, 924.

Synthesis of Complex $[NiL^1(H_2O)_3]Br_2\cdot H_2O$ (2). Complex **2** has been prepared following the same procedure as that for **1**, where $NiBr_2\cdot xH_2O$ (0.437g, 2 mmol) was used in place of NiI_2. The resulting green solution was filtered and kept in a $CaCl_2$ desiccator. A few days later green single crystals were obtained that were suitable for X-ray data collection. Yield: 70%. Anal. Calcd for $C_{13}H_{27}N_3O_5Br_2Ni$: C, 29.8; H, 5.19; N, 8.02; Ni, 11.16. Found: C, 29.72; H, 5.24; N, 7.98; Ni, 11.08. UV−vis−near-IR (methanol, nm): λ_{max} = 381, 627, 751, 924.

Synthesis of Complex $[NiL^1(H_2O)_3]Cl_2\cdot 2H_2O$ (3). Complex **3** was prepared by adopting the same procedure as that for **1** using $NiCl_2\cdot 6H_2O$ (0.475g, 2 mmol) in place of NiI_2. X-ray-suitable green crystals of complex **3** were obtained from the resulting solution after 1 week. Yield: 73%. Anal. Calcd for $C_{13}H_{29}N_3O_6Cl_2Ni$: C, 34.47; H, 6.45; N, 9.28, Ni, 12.91. Found: C, 34.41; H, 6.53; N, 9.22; Ni, 12.83. UV−vis−near-IR (methanol, nm): λ_{max} = 379, 646, 761, 971.

Detection of Hydrogen Peroxide in the Catalytic Reactions. The formation of H_2O_2 during the catalytic reaction was detected by following the development of the characteristic band for I_3^- spectrophotometrically (λ_{max} = 353 nm; ε = 26000 M^{-1} cm^{-1}), upon reaction with I^-.[16,17] The oxidation reactions of 3,5-DTBC in the presence of different catalysts were carried out as in the kinetic experiments ([complex] = 2.5 × 10^{-5} M; [3,5-DTBC] = 50 × 10^{-5} M). After 1 h of reaction, an equal volume of water was added, and the quinone formed was extracted three times with dichloromethane. The aqueous layer was acidified with H_2SO_4 to pH 2 to stop further oxidation, and 1 mL of a 10% solution of KI and 3 drops of a 3% solution of ammonium molybdate were added. In the presence of hydrogen peroxide occurs the reaction $H_2O_2 + 2I^- + 2H^+ \rightarrow 2H_2O + I_2$, and with an excess of iodide ions, the triiodide ion is formed according to the reaction $I_2(aq) + I^- \rightarrow I_3^-$. The reaction rate is slow but increases with increasing concentrations of acid, and the addition of an ammonium molybdate solution renders the reaction almost

dx.doi.org/10.1021/ic401819t | *Inorg. Chem.* 2013, 52, 13442−13452

Table 1. Crystallographic Data and Processing Parameters of Complexes 1−3

	1	2	3
empirical formula	$C_{13}H_{27}I_2N_3NiO_5$	$C_{13}H_{27}Br_2N_3NiO_5$	$C_{13}H_{29}Cl_2N_3NiO_6$
fw	617.87	523.87	452.98
system	monoclinic	monoclinic	monoclinic
space group	$P2_1/n$	$P2_1/c$	$P2_1/c$
a (Å)	9.5132(9)	9.4906(9)	9.5733(9)
b (Å)	12.5144(13)	15.7080(14)	15.4155(14)
c (Å)	17.8254(18)	13.7970(13)	13.9557(12)
α (deg)	90	90	90
β (deg)	101.734(16)	109.536(14)	109.816(14)
γ (deg)	90	90	90
V (Å^3)	2077.8(4)	1938.4(4)	1937.6(3)
Z	4	4	4
T (K)	100(2)	100(2)	100(2)
μ (mm^{-1})	3.931	5.150	1.310
D_{calc} (Mg m^{-3})	1.975	1.795	1.553
data collected	16193	14784	15136
unique reflns/R_{int}	4236/0.0313	3889/0.0275	3940/0.0253
param/restraints	247/10	247/10	262/12
GOF on F^2	1.186	1.034	1.079
R1/wR2 (all data)	0.0362/0.0781	0.0239/0.0605	0.0261/0.0679
residual extrema (e Å^{-3})	1.10/−0.63	0.63/−0.42	0.37/−0.35

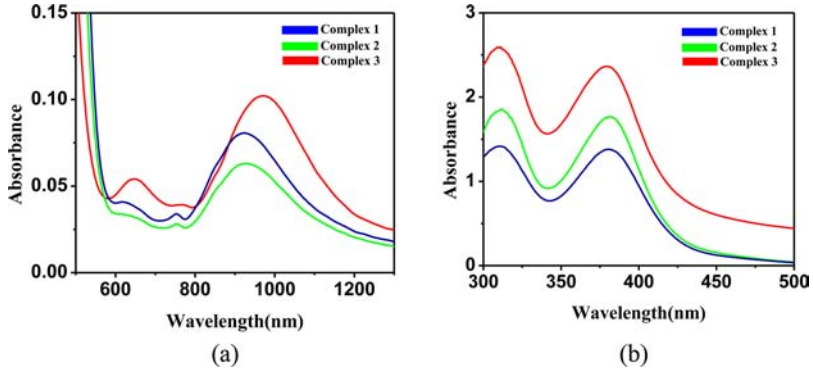

Figure 1. UV−vis spectra of (a) a 10^{-2} M solution and (b) a 10^{-3} M solution of complexes 1−3 in a methanol medium.

instantaneous. The formation of I_3^- could be monitored spectrophotometrically because of the development of the characteristic I_3^- band (λ_{max} = 353 nm; ε = 26000 M^{-1} cm^{-1}).[18]

X-ray Crystal Structure Analysis. The X-ray single-crystal data of complexes 1−3 were collected on a Bruker-AXS SMART CCD diffractometer. The crystallographic data, conditions retained for the intensity data collection, and some features of the structure refinements are listed in Table 1. The intensities were collected with Mo Kα radiation (λ = 0.71073 Å). Data processing, Lorentz polarization, and absorption corrections were performed using the *SAINT*, *SMART*, and *SADABS* computer programs.[19] The structures were solved by direct methods and refined by full-matrix least-squares methods on F^2, using the *SHELXTL*[20] program package. All non-hydrogen atoms were refined anisotropically. The hydrogen atoms were located from difference Fourier maps, assigned with isotropic displacement factors, and included in the final refinement cycles by use of either geometrical constraints (HFIX for hydrogen atoms with parent carbon atoms) or restraints (DFIX for hydrogen atoms with parent nitrogen or oxygen atoms). Molecular plots were performed with the *Mercury*[21] program, and the *PLATON*[22] program package was used for hydrogen-bonding analysis.

Potentiometric Titration. Potentiometric studies were carried out with a SYSTRONICS μ pH SYSTEM 361 pH meter fitted with blue-glass and Ag/AgCl reference electrodes, calibrated to read −log [H$^+$] directly, designated as the pH in methanol/water (90:10, v/v). In a typical titration experiment, 10 mL of a 1 × 10^{-4} M complex solution was prepared and a 0.1 M KOH solution was used as the titrant. The ionic strength was maintained with a 0.1 M KCl solution. The temperature was measured before and after each experiment and remained constant at a value of 298 ± 0.5K. Absorbances at different pH values were recorded using a Shimadzu UV-3101PC spectrophotometer. pK_a values were calculated following the literature procedure.[23]

Theoretical Methods. The geometries and energies of all complexes included in this study were computed at the BP86-D3/def2-TZVPD level of theory within the program *TURBOMOLE*, version 6.4.[24] The solvent effects were taken into account by using the COSMO (Conductor like Screening Model) solvation model.[25] For the calculations, we used the BP86 functional with the latest available correction for dispersion (D3). The orbital and spin density plots were performed at the B3LYP/6-31+G* level of theory by means of the *Gaussian 09* package.[26]

3. RESULTS AND DISCUSSION

Syntheses and FT-IR and UV−Vis Spectra of the Complexes. The Schiff-base ligand (L^1) is prepared through the classical method where salicylaldehyde and *N*-(2-aminoethyl)piperazine is refluxed in a methanol medium for 0.5 h. This ligand is further treated with nickel(II) chloride/bromide/iodide in situ separately to prepare complexes 1−3,

dx.doi.org/10.1021/ic401819t | Inorg. Chem. 2013, 52, 13442−13452

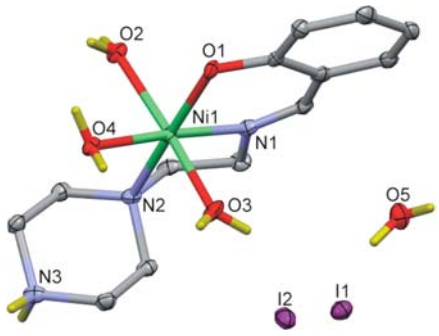

Figure 2. Perspective view (50% probability ellipsoids) of complex **1** with the atom numbering scheme.

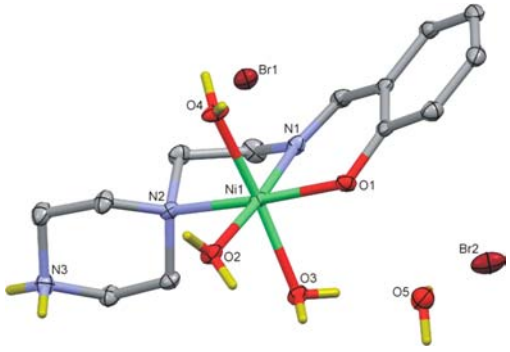

Figure 3. Perspective view (50% probability ellipsoids) of complex **2** with the atom numbering scheme.

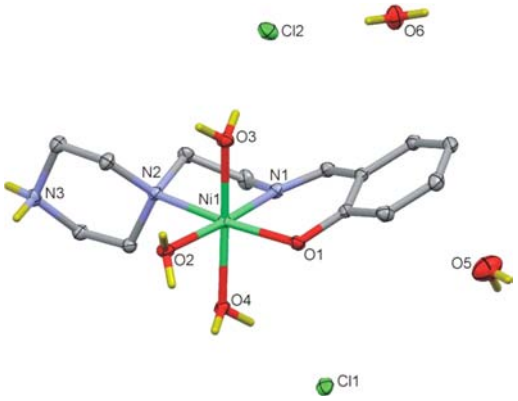

Figure 4. Perspective view (50% probability ellipsoids) of complex **3** with the atom numbering scheme.

respectively. All three complexes are characterized by routine physicochemical techniques as well as by X-ray single-crystal structure analyses. All of the complexes show IR bands due to C═N stretching in the range 1640−1650 cm^{-1} and skeleton vibrations in the range 1590−1600 cm^{-1}. A broad band in the range 3300−3500 cm^{-1} is due to a hydrogen-bonded O−H group of a coordinated water molecule (Supporting Information, Figures S1−S3). Magnetic susceptibility measurements (μ_{eff} = 3.2 μ_B at 298 K) suggest that nickel(II) possesses octahedral configuration in all three complexes. Electronic spectra (Figure 1) recorded in methanol also reveal that the coordination environment around nickel(II) in each case is roughly octahedral.[27,28] Complexes **1** and **2** display three weak absorption bands at ∼625, ∼750, and ∼925 nm (ε/dm^3 mol^{-1} cm^{-1}, 3−10) assigned to spin-allowed $^3A_{2g} \rightarrow {}^3T_{1g}(P)$, $^3A_{2g} \rightarrow {}^3T_{1g}(F)$, and $^3A_{2g} \rightarrow {}^3T_{2g}(F)$ transitions, respectively, expected for octahedral d^8 ions. In the case of complex **3**, all three bands are red-shifted with slightly higher ε values. Complexes **1**−**3** also exhibit two highly intense bands at the regions ∼310 nm (ε/dm^3 mol^{-1} cm^{-1}; 1417, 1842, and 2589 for **1**−**3**, respectively) and ∼380 nm (ε/dm^3 mol^{-1} cm^{-1} = 1384, 1762, and 2372 for **1**−**3**, respectively) most likely due to ligand-to-metal charge transfer. Solid-state electronic spectra of complexes **1**−**3** are very similar compared to their respective electronic spectrum in methanol, suggesting retention of the octahedral geometry in the solid state (Supporting Information, Figure S4).

Table 2. Selected Bond Lengths (Å) and Angles (deg) for Compounds 1−3

Complex 1			
Ni1−N1	1.994(4)	Ni1−N2	2.249(4)
Ni1−O1	2.030(3)	Ni1−O2	2.099(3)
Ni1−O3	2.076(3)	Ni1−O4	2.078(3)
N1−C7	1.273(6)	O1−C1	1.333(5)
N1−Ni1−O1	90.43(14)	O3−Ni1−O2	169.83(12)
N1−Ni1−O3	90.03(14)	O4−Ni1−O2	84.87(12)
O1−Ni1−O3	89.82(13)	N1−Ni1−N2	82.30(14)
N1−Ni1−O4	176.08(14)	O1−Ni1−N2	171.26(13)
O1−Ni1−O4	90.08(12)	O3−Ni1−N2	95.02(14)
O3−Ni1−O4	86.08(12)	O4−Ni1−N2	97.50(13)
N1−Ni1−O2	99.05(14)	O2−Ni1−N2	90.77(13)
O1−Ni1−O2	85.56(12)		
Complex 2			
Ni1−N1	2.0072(19)	Ni1−N2	2.1998(19)
Ni1−O1	2.0307(16)	Ni1−O2	2.0621(16)
Ni1−O3	2.0700(16)	Ni1−O4	2.0723(16)
N1−C7	1.276(3)	O1−C1	1.320(3)
N1−Ni1−O1	90.04(7)	O2−Ni1−O4	86.40(7)
N1−Ni1−O2	174.87(7)	O3−Ni1−O4	170.31(6)
O1−Ni1−O2	94.64(6)	N1−Ni1−N2	82.94(7)
N1−Ni1−O3	98.05(7)	O1−Ni1−N2	172.98(7)
O1−Ni1−O3	88.10(6)	O2−Ni1−N2	92.38(7)
O2−Ni1−O3	84.23(6)	O3−Ni1−N2	92.94(7)
N1−Ni1−O4	91.49(7)	O4−Ni1−N2	89.87(7)
O1−Ni1−O4	90.24(7)		
Complex 3			
Ni1−N1	1.9988(14)	Ni1−N2	2.2186(13)
Ni1−O1	2.0491(11)	Ni1−O2	2.0635(12)
Ni1−O3	2.0837(12)	Ni1−O4	2.0993(12)
N1−C7	1.278(2)	O1−C1	1.3322(19)
N1−Ni1−O1	89.12(5)	O2−Ni1−O4	84.16(5)
N1−Ni1−O2	175.04(5)	O3−Ni1−O4	172.64(5)
O1−Ni1−O2	95.81(5)	N1−Ni1−N2	82.45(5)
N1−Ni1−O3	89.96(5)	O1−Ni1−N2	171.57(5)
O1−Ni1−O3	88.71(5)	O2−Ni1−N2	92.62(5)
O2−Ni1−O3	89.54(5)	O3−Ni1−N2	91.21(5)
N1−Ni1−O4	96.64(5)	O4−Ni1−N2	92.89(5)
O1−Ni1−O4	88.13(5)		

Description of the Crystal Structures of 1−3. Perspective views together with the atom numbering schemes for complexes **1**−**3** are presented in Figure 2−4, respectively, and selected bond parameters are given in Table 2. The structures consists of mononuclear $[Ni(C_{13}H_{19}N_3O)(H_2O)_3]^{2+}$ complex cations, two halide counteranions, and lattice water

dx.doi.org/10.1021/ic401819t | Inorg. Chem. 2013, 52, 13442−13452

Table 3. Hydrogen-Bonding System for Compounds 1−3

D−H···A[a]	symmetry of A	D···A (Å)	D−H···A (deg)
	Complex **1**		
N3−H90···O5	[−x + 1, y, z]	2.720(5)	143(4)
N3−H91···I1	[−x + 1/2, y + 1/2, z − 1/2]	3.557(4)	163(4)
O2−H92···I1	[x − 1/2, −y + 3/2, z − 1/2]	3.521(3)	163(4)
O2−H93···O1	[−x, −y + 2, −z]	2.685(4)	174(5)
O3−H94···I2	[−x + 1/2, y + 1/2, −z + 1/2]	3.443(3)	166(4)
O3−H95···I1		3.438(3)	169(3)
O4−H96···I2	[−x+1/2, y + 1/2, −z + 1/2]	3.542(3)	168(3)
O4−H97···O1	[−x, −y + 2, −z]	2.696(4)	156(4)
O5−H98···I1		3.509(4)	147(4)
O5−H99···I2	[−x + 3/2, y + 1/2, −z + 1/2]	3.524(4)	175(4)
	Complex **2**		
N3−H90···Br1	[−x, y − 1/2, −z + 1/2]	3.175(2)	167(2)
N3−H91···Br2	[−x + 1, y − 1/2, −z + 1/2]	3.312(2)	166(2)
O2−H92···O1	[−x + 1, −y, −z + 1]	2.754(2)	151.6(19)
O2−H93···Br1	[−x, −y, −z + 1]	3.4685(18)	156(2)
O3−H94···O1	[−x + 1, −y, −z + 1]	2.751(2)	168(3)
O3−H95···O5		2.722(3)	173(2)
O4−H96···Br1		3.2871(18)	176(2)
O4−H97···Br2	[x − 1, y, z]	3.2639(18)	172(2)
O5−H98···Br2		3.2812(19)	160(3)
O5−H99···Br1	[−x + 1, −y, −z + 1]	3.3511(19)	161(2)
	Complex **3**		
N3−H90···Cl2	[−x, y − 1/2, −z + 1/2]	3.2551(16)	155.9(17)
N3−H91···O6	[−x, −y, −z]	2.709(2)	149.9(16)
O2−H92···Cl1	[−x + 1, −y, −z + 1]	3.1576(14)	161.5(18)
O2−H93···O1	[−x + 1, −y, −z + 1]	2.7069(17)	168.6(16)
O3−H94···Cl1	[x − 1, y, z]	3.1260(14)	167(2)
O3−H95···Cl2		3.0918(13)	170.8(18)
O4−H96···Cl1		3.1823(14)	164.0(18)
O4−H97···O1	[−x + 1, −y, −z + 1]	2.7016(16)	164.7(19)
O5−H98···Cl2	[x + 1, −y + 1/2, z + 1/2]	3.2295(19)	1592)
O5−H99···Cl1	[x, −y + 1/2, z + 1/2]	3.1961(18)	168(3)
O6−H100···Cl2		3.2166(15)	157(2)
O6−H101···Cl1	[−x + 1, y + 1/2, −z + 1/2]	3.2145(15)	170(3)

[a]D = donor; A = acceptor.

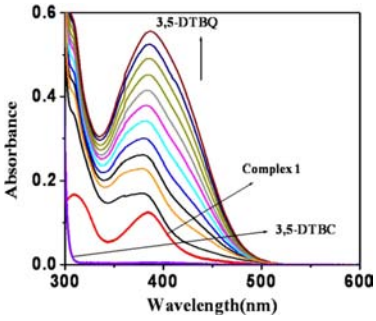

Figure 5. UV−vis spectra of (i) complex **1** and (ii) 3,5-DTBC and (iii) changes in the UV−vis spectra of complex **1** upon the addition of 3,5-DTBC observed after each 5 min interval.

molecules (one in the case of complexes **1** and **2** and two water molecules in the case of **3**). The nickel(II) centers are ligated by N1, N2, and O1 donor atoms of the $C_{13}H_{19}N_3O$ ligand and three aqua ligands in a distorted octahedral environment with

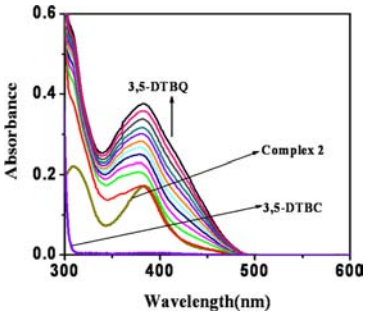

Figure 6. UV−vis spectra of (i) complex **2** and (ii) 3,5-DTBC and (iii) changes in the UV−vis spectra of complex **2** upon the addition of 3,5-DTBC observed after each 5 min interval.

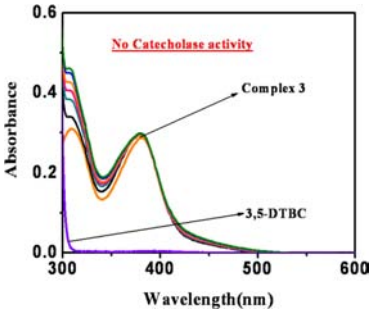

Figure 7. UV−vis spectra of (i) complex **3** and (ii) 3,5-DTBC and (iii) changes in the UV−vis spectra of complex **3** upon the addition of 3,5-DTBC observed after each 5 min interval.

Table 4. Kinetic Parameters for Complexes 1 and 2

catalyst	V_{max} (M s^{-1})	K_M (M)	k_{cat} (h^{-1})
1	2.5747×10^{-6}	1.1053×10^{-4}	9.2689×10^{1}
2	2.3562×10^{-6}	0.88159×10^{-4}	8.4825×10^{1}

mer conformation. The Ni−N1, Ni−N2, Ni−O1, and Ni−O_{aq} bond distances vary in the ranges 1.994(4)−2.0072(19), 2.1998(19)−2.249(4), 2.030(3)−2.0491(11), and 2.0621(16)−2.0993(12) Å, respectively. The mean N1−Ni−O1, N1−Ni−N2, and O1−Ni−N2 bond angles are 89.86, 82.56, and 171.93°, respectively. The piperazine moieties adopt chair conformation. The N3 atoms are not ligated to the nickel(II) center but form hydrogen bonds to one halide anion and one water molecule in the case of complexes **1** and **3** and to two bromide anions in the case of complex **2** (Table 2). In addition, the three aqua ligands and the lattice water molecules form hydrogen bonds of the types O−H···X and O−H···O to generate supramolecular network structures (Table 3 and Supporting Information, Figures S5−S7).

Catechol Oxidase Activity. In order to confirm the ability of the nickel(II) complexes to oxidize 3,5-DTBC, 1×10^{-4} mol dm^{-3} methanolic solutions of **1**−**3** were treated with 1×10^{-2} mol dm^{-3} (100 equiv) of 3,5-DTBC under aerobic conditions. The course of the reaction was followed by UV−vis spectroscopy, and the time-dependent spectral scans of the three complexes are depicted in Figures 5−7. From the figures, it is evident that a band ∼390 nm is observed to increase with time after the addition of 3,5-DTBC because of the gradual increment of the concentration of 3,5-DTBQ (3,5-DTBQ exhibits λ_{max} ∼ 400 nm in methanol) in the cases of **1**- and **2**-catalyzed reactions, whereas nearly no change is noticed in the spectral pattern with complex **3**. These data unambiguously

dx.doi.org/10.1021/ic401819t | Inorg. Chem. 2013, 52, 13442−13452

Table 5. Kinetic Data for Catecholase-like Activity of Different Mono- and Dinuclear Copper and Nickel Complexes

catalyst[a]	solvent	k_{cat} (h^{-1})	ref (year)
Mononuclear Ni(II) Compounds			
(1) $[NiL^2(H_2O)_3](NO_3)_2$	methanol	52.60	15 (2012)
Dinuclear Ni(II) Compounds			
(2) $[Ni_2(L^1)_2(NCS)_2]$	acetonitrile	64.1	29 (2012)
Mononuclear Cu(II) Compounds			
(3) $[Cu(L^7)Cl]Cl$	methanol	11.16	30 (2011)
Dinuclear Cu(II) Compounds			
(4) $[Cu_2(H_2L)(\mu\text{-}OH)](ClO_4)_2$	methanol	28.74	31 (2008)
(5) $[Cu_2L_2(ClO_4)_2]$	methanol	93.6	32 (2012)
(6) $[Cu_2(L^{H,H}\text{–}O)(OH)(MeCN)_2][ClO_4]_2$	methanol	55	33 (2012)
(7) Cu_2diep	water–methanol	63	34 (2012)

[a] HL^2 (1) = 2-[(2-piperazin-1-yl-ethylimino)methyl]phenol; HL^1 (2) = 2-[1-(3-methylaminopropylamino)ethyl]phenol; HL^7 (3) = 6-(bis-pyrazol-1-ylmethylamino)hexan-1-ol; H_3L (4) = 2,6-bis[{{(2-hydroxybenzyl)(*N*′,*N*′-(dimethylamino)ethyl)}amino}methyl]-4-methylphenol; HL (5) = 2-[[2-(diethylamino)ethylamino]methyl]-phenol; $L^{H,H}$ (6) = 1,3-bis[(*N*,*N*-dimethylaminoethyl)aminomethyl]-benzene; diep (7) = 2,8-dimethyl-5,11-bis(pyridin-2-ethyl)-1,4,5,6,7,10,11,12-octahydroimidazo[4,5-*h*]imidazo[4,5-*c*][1,6]-diazecine.

demonstrate that **1** and **2** are active catalysts for the aerial oxidation of 3,5-DTBC to 3,5-DTBQ, whereas **3** turns out to be inactive. The inactivity of complex **3** is apparently quite surprising because structure analyses reveal that all three complexes have very similar structural features in the solid state. It is now quite urgent to know whether the observed solid-state structures remain intact in solution. In order to get an idea regarding the solution structure of the complexes, we first of all performed a conductivity study of them in methanol (vide infra). The kinetics of the 3,5-DTBC oxidation was determined by monitoring the increase of the concentration of the product 3,5- DTBQ. The kinetics for the oxidation of the substrate 3,5-DTBC was determined by the initial rate method at 25 °C. The concentration of the substrate 3,5-DTBC was always kept 10 times higher than that of the complex, and the increase of the respective quinone concentration was determined at 390 nm wavelength for each complex. Solutions of substrates of concentration ranging from 0.001 to 0.05 mol dm^{-3} were prepared from a concentrated stock solution in methanol. A total of 2 mL of the substrate solution was poured into a 1 cm spectrophotometer quartz cell thermostatted at 25 °C. Then 0.04 mL of a 0.005 mol dm^{-3} complex solution was quickly added to it so that the ultimate concentration of the complex became 1×10^{-4} mol dm^{-3}. The dependence of the initial rate on the concentration of the substrate was spectrophotometrically monitored at the respective wavelength. Moreover, the initial rate method showed a first-order dependence on the complex concentration and exhibited saturation kinetics at higher substrate concentrations. Because both complexes **1** and **2** showed saturation kinetics, a treatment based on the Michaelis–Menten model seemed to be appropriate. The binding constant (K_M), maximum velocity (V_{max}), and rate constant for dissociation of the substrates (i.e., turnover number, k_{cat}) were calculated for the complexes using the Lineweaver–Burk graph of $1/V$ versus $1/[S]$ (Supporting Information, Figures S8–S10), with the equation $1/V = (K_M/V_{max})(1/[S]) + 1/V_{max}$, and the kinetic parameters are presented in Table 4. Table 5 represents the k_{cat} values of some mono- and dinuclear complexes of copper(II) and

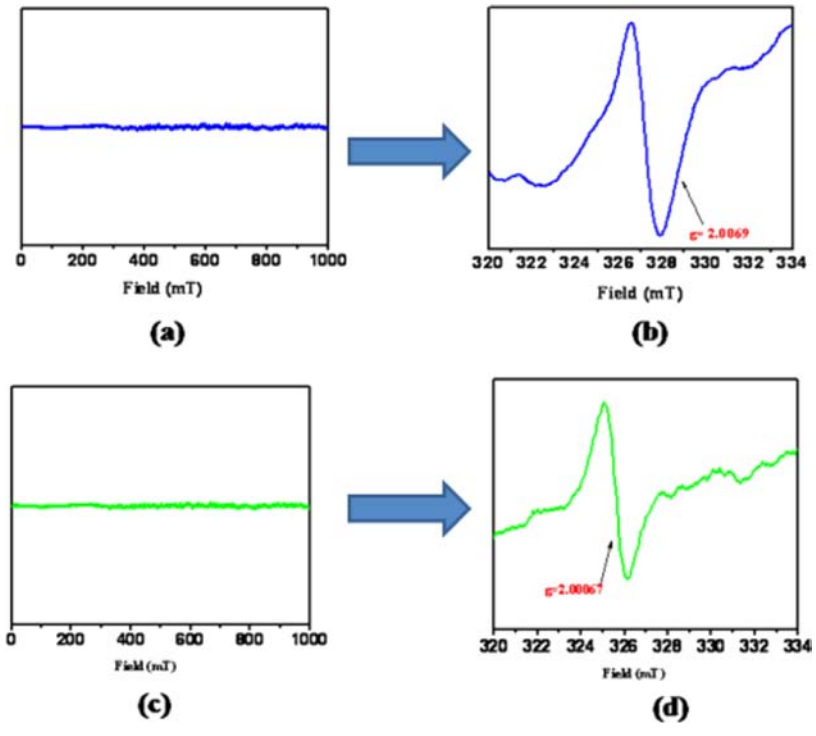

Figure 8. EPR spectra of (a) complex **1**, (b) a mixture of complex **1** and 3,5-DTBC, (c) complex **2**, and (d) a mixture of complex **2** and 3,5-DTBC.

dx.doi.org/10.1021/ic401819t | *Inorg. Chem.* 2013, 52, 13442–13452

Table 6. E° Values in CV and DPV for Complexes 1−3

complex	E°/E_{peak} values from CV	E° values from DPV
3	0.97,[a] 1.25,[a] 1.6,[a] −1.10 (220),[b] −1.53 (120)[b]	0.89, 1.16, 1.3, 1.5, −1.14, −1.51, −2.0
2	0.95, 1.19 (90),[b] 1.45, −1.15 (160),[b] −1.44 (250)[b]	0.8, 1.13, 1.38, −1.14, −1.56, −2.0
1	0.5,[a] 0.75 (200), 1.05,[a] −1.17 (200),[b] −1.51 (200)[b]	0.4, 0.76, 1.1, −1.23, −2.0

[a]Irreversible. [b]E°/V (ΔE_p/mV), where $\Delta E_p = E_{pa} - E_{pc}$

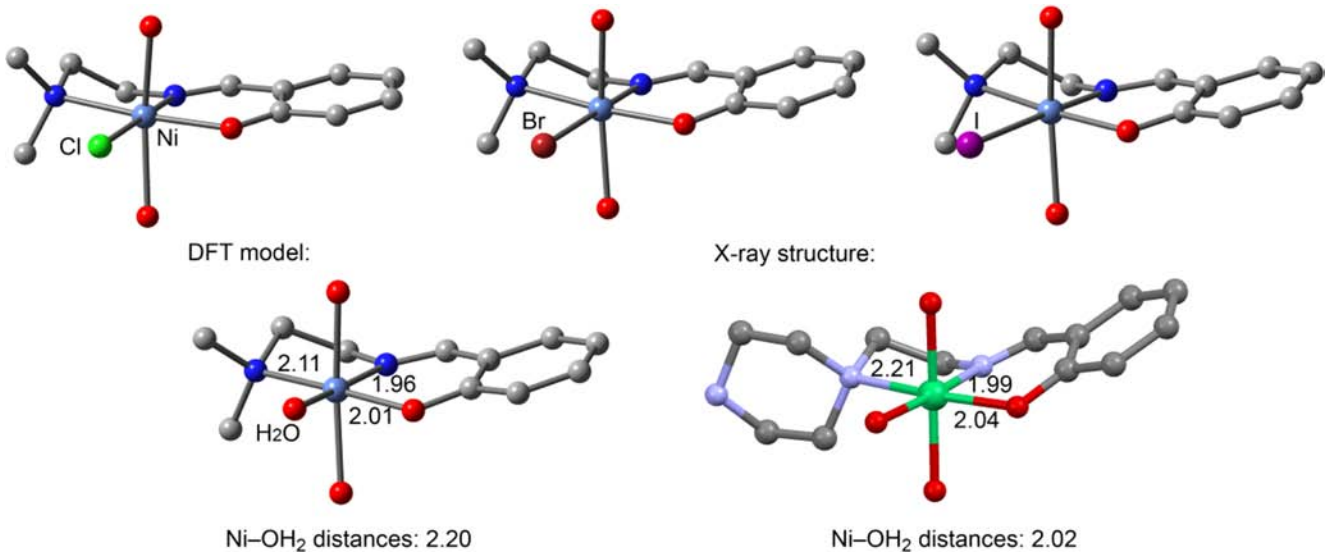

Figure 9. Bottom: DFT model and X-ray structure of compound **1**. Top: optimized structures of $[NiLX(OH_2)_2]$ complexes (X = Cl, Br, and I; left, middle, and right, respectively).

Scheme 2. Reaction Used To Evaluate the Substitution Ability of the Halides

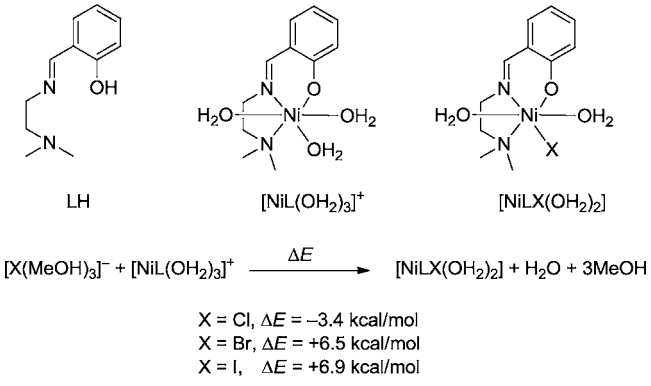

Scheme 3. Proposed Catalytic Cycle of the Oxidation of 3,5-Dimethylcatechol by the $[NiL(OH_2)_3]^+$ Complex

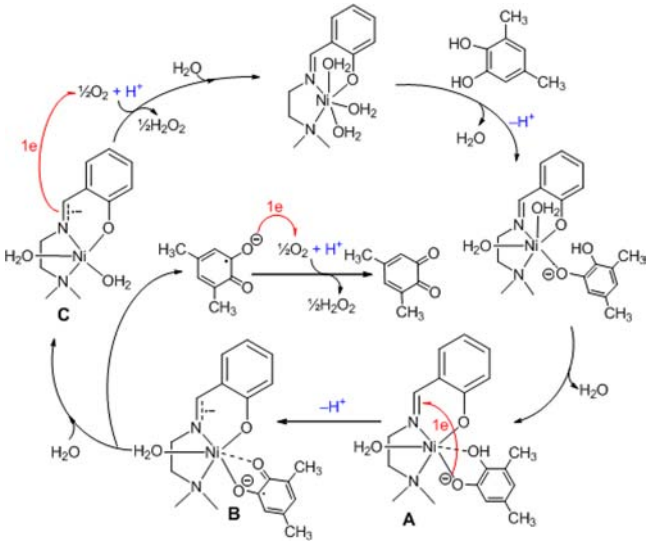

nickel(II) reported recently. Upon comparison of Tables 4 and 5, it may be stated that complexes **1** and **2** belong to the highly efficient catalyst group, where the order of their activity is **1** > **2**.

Here it is noted that the catalytic reaction performed under an inert atmosphere does not show the occurrence of 3,5-DTBQ. However, the formation of 3,5-DTBQ was immediately detected upon exposure of the reaction mixture to a dioxygen atmosphere. It is now essential to know whether dioxygen reduces to water or H_2O_2 during the oxidation process. The oxidation of I^- to I_2 followed by the generation of I_3^-, as is evident from the UV−vis spectral study of the solution (Supporting Information, Figure S11) obtained after proper workup of the mixture of catechol, complex, and KI (see the Experimental Section), clearly hints that dioxygen is reduced to H_2O_2, as reported by other investigators also.[29,35]

Conductivity Study. To rationalize the composition of the complexes in solution, a molar conductivity study of the 10^{-3} M methanolic solution of complexes **1**−**3** has been performed. The conductance values at 298 K for complexes **1**−**3** are 175, 165, and 110 Ω^{-1} cm^2 M^{-1}, respectively. Critical analysis of the values suggests that complex **3** behaves as a 1:1 electrolyte, whereas complexes **1** and **2** behave as a 2:1 electrolyte, as expected from their solid-state structure (vide supra). The 1:1 electrolytic behavior of complex **3** may be rationalized by considering that in solution one Cl^- ion remains in the outer

dx.doi.org/10.1021/ic401819t | Inorg. Chem. 2013, 52, 13442−13452

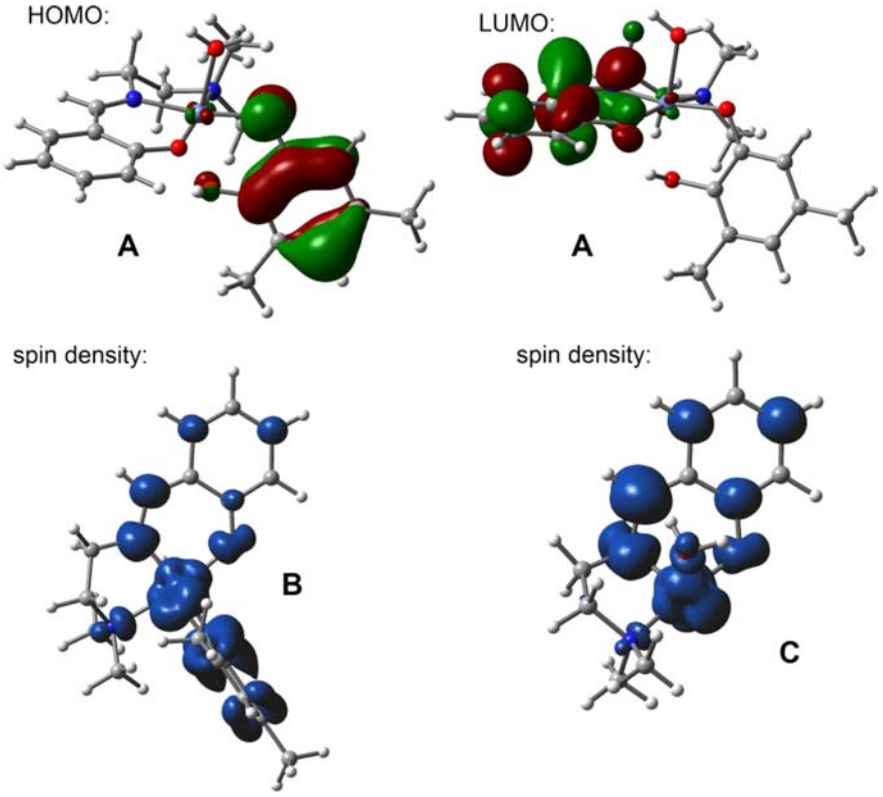

Figure 10. HOMO and LUMO of **A** and spin densities in **B** and **C** computed at the UB3LYP/6-31+G* level of theory.

sphere whereas the other one coordinates with the nickel(II) center. It is now reasonable to consider that the affinity to make the metal−substrate complex in the case of complex **3** is less because one Cl^- is in the coordination sphere, which leads to neutralization of the effective positive charge on nickel(II) to a greater extent compared to complexes **1** and **2**, where the counteranions are in the outer sphere in solution also. The direct effect is the ineffectiveness of **3** in catalyzing the oxidation of 3,5-DTBC. Now it is essential to know the most probable reason behind the activity of the complexes to catalyze the oxidation of 3,5-DTBC, i.e., whether metal-centered redox participation or a radical pathway is responsible for that activity, and for that purpose, we have performed EPR and CV studies.

EPR Study. The EPR study was performed at 77 K temperature under a 9.13 GHz magnetic field immediately after mixing 3,5-DTBC with a 10^{-3} M methanolic solution of complexes **1** and **2** in an inert atmosphere. The EPR study reveals that the complexes are EPR-inactive, whereas a sharp signal at $g \sim 2$ (Figure 8) is generated when the spectra are taken after the addition of 3,5-DTBC to the bromide and iodide complexes, suggesting the formation of a free radical.[29,36,37] However, under the experimental conditions, the free ligand and 3,5-DTBC mixture or nickel salt and 3,5-DTBC mixture are EPR-silent. This implies that oxidation of 3,5-DTBC is occurring via a radical pathway only when nickel complexes are used as catalysts. The generation of a ligand-centered radical has further been established by the DFT study.

CV Study. All complexes show ligand-centered oxidation at 0.70−1.0 V, with the oxidations being irreversible for the chloro and bromo complexes and quasi-reversible for the iodo complex. At around 1.1−1.2 V, the oxidative response is probably due to nickel(II) to nickel(III) oxidation, which shows quasi-reversible behavior for the bromo complex but behaves irreversibly for the other two complexes. The oxidative waves at 0.4 V for the iodo complex, 1.4 V for the bromo complex, and 1.3−1.5 V for the chloro complex probably correspond to halide oxidations (X^- to $^1/_2X_2$).

On the negative side of the reference electrode, two quasi-reversible reductions are observed at −1.1 to −1.2 V and at −1.4 to −1.5 V. The first reduction process is undoubtedly ligand-centered, which is conclusively supported by the DFT calculations (vide infra). The second reduction is also probably a ligand-based process, although nickel(II)/nickel(I) reduction cannot be ruled out at this potential. At more negative potential at −2.0 V, another reductive peak with a large current height is observed in DPV, which is again assigned to ligand-centered reduction. The CV and DPV data are summarized in Table 6, and figures are given in the Supporting Information (Figures S12−S14).

DFT Study. As aforementioned, three new complexes have been synthesized and X-ray characterized (see Scheme 1). Moreover, it has been demonstrated that complex **1** shows very high catecholase activity and complex **2** is moderately active. In sharp contrast, complex **3** is totally inactive in catalyzing the aerobic oxidation of DTBC. X-ray single-crystal structure determination reveals that all complexes are cationic nickel(II) complexes with two halides as counteranions.

Interestingly, conductance measurement of the three complexes in methanol suggests that complexes **1** and **2** behave as a 2:1 electrolyte, as expected accordingly to the solid-state structure. However, the conductance measurement for complex **3** agrees with the formation of a 1:1 electrolyte, suggesting that in methanol solution one Cl^- ion is coordinated with the nickel metal center (vide supra). Therefore, because of the presence of chloride coordinated to the metal in solution, DTBC is not able to approach the metal and consequently the

dx.doi.org/10.1021/ic401819t | *Inorg. Chem.* 2013, 52, 13442−13452

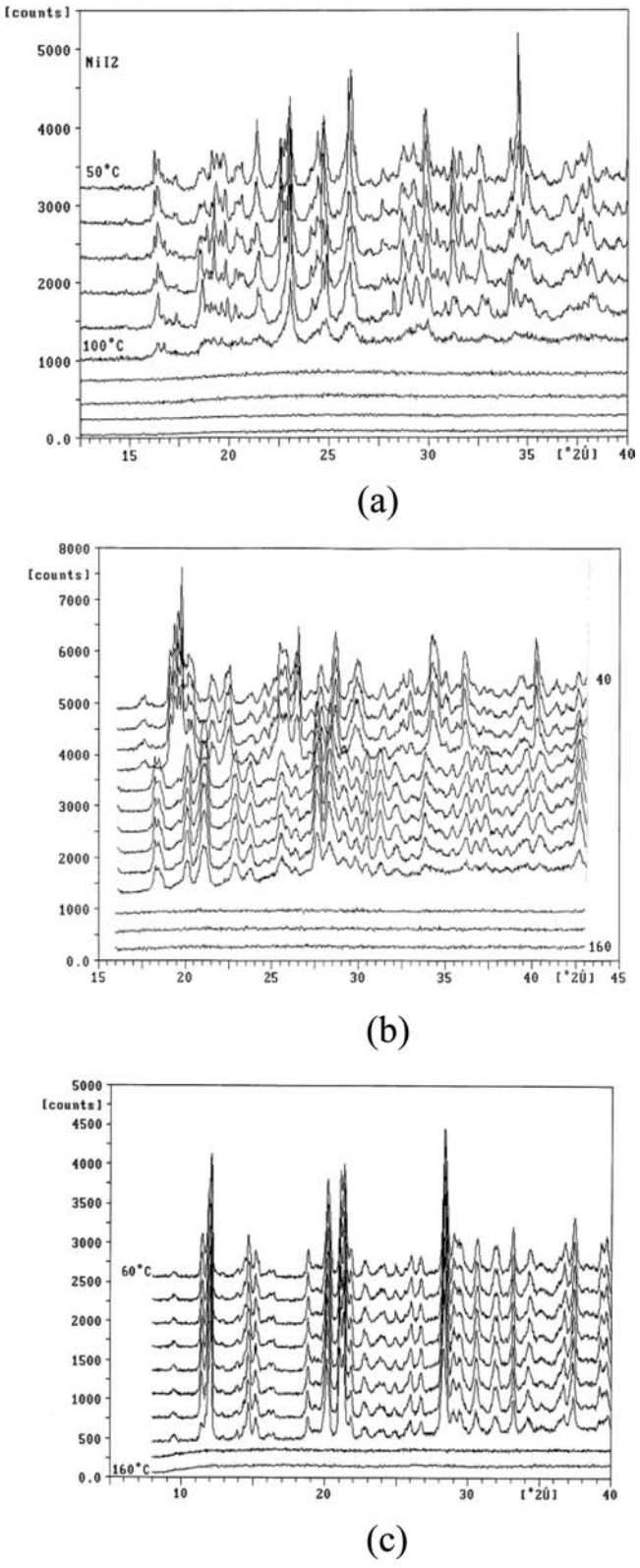

Figure 11. Variable-temperature PXRD pattern of complexes (a) **1**, (b) **2**, and (c) **3**.

chloride complex does not show catecholase activity. We have performed a DFT study in order to verify this hypothesis. We have used the BP86-D3 functional and def2-TZVPD basis set for the study (see the Theoretical Methods section for details). We have used a theoretical model in which we have reduced the size of the ligand, as represented in Figure 9 and Scheme 2. In the DFT model, we have used a dimethylamino group instead of the protonated piperazine residue (LH; see Scheme 2). It can be observed that the optimized structure is very similar to the solid-state geometry. The computed equatorial metal–ligand distances agree well with the experimental ones. The Ni–OH_2 distances are slightly larger in the theoretical model than in the X-ray structure. We have also optimized the complexes by replacing one water molecule by a chloride, bromide, or iodide anion, and the geometries are shown in the top part of Figure 9. We have replaced the equatorial water molecule by the halide because this is the substitution that yields the most stable complex. These complexes have been used to evaluate the energetic cost of replacing one water molecule by the halide. It should be mentioned that the calculation in the gas phase gives very favorable energies for this substitution because of the strong electrostatic attraction between the positive metal center and the corresponding counterion. However, when solvent effects are taken into account, the results are very different. In particular, we have used three explicit solvent molecules in conjunction with a continuum model using COSMO mimicking methanol as the solvent. The results are shown in Scheme 2, and it can be observed that only the chloride anion is able to substitute the equatorial water molecule of the complex, while the other two halides are not able to do this substitution. This likely explains the formation of a 1:1 electrolyte in a methanol solution of this complex, where one Cl^- ion is coordinated to the nickel metal center, preventing the DTBC approach to the metal.

Theoretical Study of the Catecholase Mechanism of the Nickel Complex. It is well established that catechol may bind with metal in different modes of coordination where monodentate and chelated bidentate modes (considering a single metal center) are more common. Here, the important issue is which mode of catechol binding is happening in our case. The pK_a values of the substrate and those of the complexes may be useful to address that issue. The pK_a values of 3,5-DTBC are reported as 10.4 and 14.7.[34,35,38] Complexes **1** and **2** exhibit pK_a values of 5.9 and 5.93 for first M–OH_2(1) and 8.67 and 8.73 for second M–OH_2(2), respectively (Supporting Information, Figure S15). The above data clearly demonstrate that at the experimental conditions deprotonation of a second water molecule of **1** and **2** is not feasible. So, a monodentate mode of catechol coordination with the nickel(II) center is more probable. The proposed mechanism for the catalytic cycle for the oxidation of 3,5-dimethylcatechol (as a model of 3,5-DTBC by the $[NiL(OH_2)_3]^+$ complex) is shown in Scheme 3. We have computed all of the intermediates involved in the cycle, and we have focused our attention on the key intermediates **A**–**C**, analyzing the frontier orbitals in **A** and spin densities in **B** and **C** in order to further confirm the mechanistic proposal. In the optimized complexes, an ancillary interaction between the nickel metal center and oxygen atom of the phenolic –OH group in **A** and the oxygen atom of the carbonyl group in **B** is observed and has been represented as a dashed line. The electron transfers are highlighted in red and the proton transfers in blue.

In Figure 10, we show the highest occupied molecular orbital (HOMO) and lowest unoccupied molecular orbital (LUMO) of compound **A**, taking into account that there are two unpaired electrons in **A** mainly located in the $d_{x^2-y^2}$ and d_{z^2} orbitals of the Ni^{2+} metal center; the HOMO that is represented corresponds to the highest-energy orbital with

dx.doi.org/10.1021/ic401819t | Inorg. Chem. 2013, 52, 13442–13452

double occupancy. Interestingly, the HOMO is located basically in the catechol ring and the LUMO in the C═N bond and the aromatic ring of the ligand (L). Therefore, the electron transfer proposed in the mechanism is supported by the orbital distribution in **A**, and likely this electron transfer is facilitated by the metal center. As a consequence, the spin-density distribution in **B** shows, on the one hand, the two unpaired electrons on the nickel metal center with some spin density delocalized into the atoms directly bonded to the nickel and, on the other hand, one unpaired electron mainly localized in the C═N bond and three carbon atoms of the aromatic ring of the ligand and the other electron delocalized in the catechol ring and oxygen atoms. This distribution agrees well with the HOMO−LUMO shape observed in **A**. Finally, in **C**, the distribution of the electron density (apart from the two electrons of nickel) is again located in the C═N bond and three aromatic carbon atoms. The C═N bond elongates from 1.30 to 1.38 Å upon electron transfer, as expected taking into consideration the antibonding nature of the LUMO.

From the above discussion, it may be stated that the electrochemical study hints that the first reduction is ligand-centered, which is confirmed by DFT studies. The EPR study clearly demonstrates the formation of a radical in the presence of 3,5-DTBC. DFT calculations support the ligand-centered radical generation. Thus, at this moment, the radical pathway is supposed to be the more probable reason for the catecholase activity of complexes **1** and **2**.

Thermogravimetric Analysis. Thermal studies of all three complexes show well-defined stepwise decomposition (Supporting Information, Figures S16−S18). Complexes **2** and **3** have similar types of thermograms, whereas complex **1** shows a slightly different type of decomposition. The loss of five water molecules present in complex **3** takes place in two consecutive steps upon heating. In first step, the weight loss is 12.2% (calcd 11.9%), and in second step, the weight loss is 7.7% (calcd 7.9%), suggesting the loss of three and two water molecules, respectively, between 27 and 199 °C. Complex **2** shows weight losses of 6.8% (calcd 6.87%) and 6.9% (calcd 6.87%), corresponding to the elimination of two water molecules in each step in the temperature range of 31−212 °C. The species obtained after the first step of deaquation of **2** and **3** via a temperature arrest technique does not show any visual color change, whereas the species generated after the second step of deaquation is red in color. The red species turns green immediately upon exposure to an open atmosphere. The color change is supposed to be due to an octahedral to square-planar structural transformation. In the case of complex **1**, single-step decomposition takes place in the temperature range of 27−185 °C. Here the weight loss is 13.14% (calcd 11.66%), which is responsible for the loss of four water molecules. In this case also, the dehydrated species is red-colored. Fortunately, this red species takes a few minutes to convert to the green species even upon exposure to an open atmosphere. The red species is diamagnetic, and solid-state electronic spectral analysis (Supporting Information, Figure S19) clearly suggests a square-planar environment around nickel(II). However, all three dehydrated species upon further heating generate NiO as the thermally stable end product (for complex **1**, expt wt loss = 88.42% at 594 °C and theor wt loss = 87.79%.; for complex **2**, expt wt loss = 80% at 595 °C and theor wt loss = 85.77%, and for complex **3**, expt wt loss = 83.7% at 585 °C and theor wt loss = 83.55%).

Variable-Temperature PXRD Study. In order to gain a better understanding of the thermal reactions of **1**−**3**, we performed a variable-temperature PXRD study (Figure 11). From the PXRD patterns, it is evident that in all cases the crystalline nature of the species remains intact up to 100 °C and after 150 °C all species become amorphous. The most interesting feature is obtained from complex **2**; the variable-temperature PXRD patterns clearly show a phase transition after 80 °C. At present, the reason of this phase transition is not clear to us. Variable-temperature FT-IR and UV−vis−near-IR spectral studies and detailed DSC analysis, which are underway with similar other systems in our laboratory, are very much essential for a better description of that phase transition. However, from the variable-temperature PXRD patterns, it is obvious that without the coordinated water molecules the crystalline nature of any of the species cannot be retained.

4. CONCLUSION

The century-old Werner's coordination theorem becomes the guideline to establish the structure−function relationship in small coordination complexes of the nickel(II) Schiff-base system demonstrated in the present work. All three nickel(II) halide complexes of a tridentate uninegative Schiff-base ligand (L^1) in the solid state have similar structures with two halide ions in the outer coordination sphere. However, in solution they exhibit different coordination chemistries. In the case of the chloride complex **3**, upon dissolution one of the chloride ions enters into the inner coordination sphere, whereas in the case of the other two complexes, the halide ions remain as counteranions. These particular features have been authenticated by classical experimental verification and, more interestingly, by DFT calculations to provide a new dimension to the present study. Because of a change in the status of the chloride ions from counteranions to coordinating ligands, effective charge neutralization of the central metal ion takes place to such an extent that enzyme−substrate adduct formation, the key step in any catalysis, is not favored and consequently complex **3** in solution does not exhibit any catalytic activity to catalyze the aerobic oxidation of 3,5-DTBC. On the other hand, the other two complexes show excellent catecholase-like activity, and a radical mechanism has been proposed to be the possible mechanistic pathway behind that oxidation on the basis of experimental observations and DFT calculations.

■ ASSOCIATED CONTENT

Supporting Information

X-ray crystallographic data in CIF format of complexes **1**−**3**, FT-IR spectra, electronic spectra in the solid state, packing diagrams, kinetic plots, electronic spectra of the formation of I_3^-, CV and DPV diagrams, spectrophotometric titration plots, and thermograms. This material is available free of charge via the Internet at http://pubs.acs.org.

■ AUTHOR INFORMATION

Corresponding Authors

*E-mail: dasdebasis2001@yahoo.com.
*E-mail: toni.frontera@uib.es.
*E-mail: mautner@tugraz.at.

Notes

The authors declare no competing financial interest.

■ ACKNOWLEDGMENTS

This work was supported by the Council of Industrial and Scientific Research, New Delhi [CSIR Project 01(2464)/11/EMR-II dated 16-05-2011 to D.D.], the DGICYT of Spain (Projects CTQ2011-27512/BQU and CONSOLIDER INGENIO 2010 CSD2010-00065, FEDER funds), and the Direcció General de Recerca i Innovació del Govern Balear (Project 23/2011, FEDER funds). F.A.M. thanks Dr. J. Baumgartner (TU-Graz) for assistance.

■ REFERENCES

(1) Ferentinos, E.; Maganas, D.; Raptopoulou, C. P.; Terzis, A.; Psycharis, V.; Robertson, N.; Kyritsis, P. *Dalton Trans.* **2011**, *40*, 169−180.
(2) Maganas, D.; Grigoropoulos, A.; Staniland, S. S.; Chatziefthimiou, S. D.; Harrison, A.; Robertson, N.; Kyritsis, P.; Neese, F. *Inorg. Chem.* **2010**, *49*, 5079−5093.
(3) Li, J.; Song, H.; Cui, C.; Cheng, J.-P. *Inorg. Chem.* **2008**, *47*, 3468−3470.
(4) Rotthaus, O.; Thomas, F.; Jarjayes, O.; Saint-Aman, C. P. E.; Pierre, J.-L. *Eur. J. Inorg. Chem.* **2006**, *12*, 6953−6962.
(5) Mukhopadhyay, S.; Mandal, D.; Ghosh, D.; Goldberg, I.; Chaudhury, M. *Inorg. Chem.* **2003**, *42*, 8439−8445.
(6) Das, D.; Ray Chaudhuri, N.; Ghosh, A. *Polyhedron* **1996**, *15*, 3919−3922.
(7) Banu, K. S.; Chattopadhyay, T.; Banerjee, A.; Bhattacharaya, S.; Suresh, E.; Nethaji, M.; Zangrando, E.; Das, D. *Inorg. Chem.* **2008**, *47*, 7083−7093.
(8) Chattopadhyay, T.; Mukherjee, M.; Mondal, A.; Maiti, P.; Banerjee, A.; Banu, K. S.; Bhattacharya, S.; Roy, B.; Chattopadhyay, D. J.; Mondal, T. K.; Nethaji, M.; Zangrando, E.; Das, D. *Inorg. Chem.* **2010**, *49*, 3121−3129.
(9) Banu, K. S.; Chattopadhyay, T.; Banerjee, A.; Mukherjee, M.; Bhattacharya, S.; Patra, G. K.; Zangrando, E.; Das, D. *Dalton Trans.* **2009**, 8755−8764.
(10) Banu, K. S.; Chattopadhyay, T.; Banerjee, A.; Bhattacharya, S.; Zangrando, E.; Das, D. *J. Mol. Catal. A: Chem.* **2009**, *310*, 34−41.
(11) Guha, A.; Banu, K. S.; Banerjee, A.; Ghosh, T.; Bhattacharya, S.; Zangrando, E.; Das, D. *J. Mol. Catal. A: Chem.* **2011**, *338*, 51−57.
(12) Guha, A.; Banerjee, A.; Mondol, R.; Zangrando, E.; Das, D. *J. Coord. Chem.* **2011**, *22*, 3872−3886.
(13) Banerjee, A.; Guha, A.; Maiti, P.; Goswami, S.; Chattopadhyay, T.; Mondal, T. K.; Bhattacharya, S.; Zangrando, E.; Das, D. *Transition Met. Chem.* **2011**, *36*, 195−199.
(14) Das, S.; Maiti, P.; Ghosh, T.; Zangrando, E.; Das, D. *Inorg. Chem. Commun.* **2012**, *15*, 266−268.
(15) Guha, A.; Banu, K. S.; Das, S.; Chattopadhyay, T.; Sanyal, R.; Zangrando, E.; Das, D. *Polyhedron* **2013**, *52*, 669−678.
(16) (a) Monzani, E.; Quinti, L.; Perotti, A.; Casella, L.; Gullotti, M.; Randaccio, L.; Geremia, S.; Nardin, G.; Faleschini, P.; Tabbi, G. *Inorg. Chem.* **1998**, *37*, 553−562. (b) Monzani, E.; Battaini, G.; Perotti, A.; Casella, L.; Gullotti, M.; Santagostini, L.; Nardin, G.; Randaccio, L.; Geremia, S.; Zanello, P.; Opromolla, G. *Inorg. Chem.* **1999**, *38*, 5359−5369.
(17) Ackermann, J.; Meyer, F.; Kaifer, E.; Pritzkow, H. *Chem.—Eur. J.* **2002**, *8*, 247−258.
(18) Monzani, E.; Quinti, L.; Perotti, A.; Casella, L.; Gullotti, M.; Randaccio, L.; Geremia, S.; Nardin, G.; Faleschini, P.; Tabbi, G. *Inorg. Chem.* **1998**, *37*, 553−562.
(19) (a) *SAINT*, version 7.23; *SMART*; Bruker AXS Inc.: Madison, WI, 2005 and 2006. (b) Sheldrick, G. M. *SADABS*, version 2; University of Göttingen, Göttingen, Germany, 2001.
(20) Sheldrick, G. M. *Acta Crystallogr.* **2008**, *A64*, 112.
(21) Macrae, C. F.; Edgington, P. R.; McCabe, P.; Pidcock, E.; Shields, G. P.; Taylor, R.; Towler, T.; van de Streek, J. *J. Appl. Crystallogr.* **2006**, *39*, 453.
(22) Spek, A. L. *Acta Crystallogr., Sect. D* **2009**, *65*, 148.
(23) Osório, R. E. H. M. B.; Peralta, R. A.; Bortoluzzi, A. J.; de Almeida, V. R.; Szpoganicz, B.; Fischer, F. L.; Terenzi, H.; Mangrich, A. S.; Mantovani, K. M.; Ferreira, D. E. C.; Rocha, W. R.; Haase, W.; Tomkowicz, Z.; Anjos, A.; Neves, A. *Inorg. Chem.* **2012**, *51*, 1569−1589.
(24) Ahlrichs, R.; Bär, M.; Hacer, M.; Horn, H.; Kömel, C. *Chem. Phys. Lett.* **1989**, *162*, 165−169.
(25) Klamt, A.; Schüürmann, G. *J. Chem. Soc., Perkin Trans. 2* **1993**, 799−805.
(26) Frisch, M. J.; Trucks, G. W.; Schlegel, H. B.; Scuseria, G. E.; Robb, M. A.; Cheeseman, J. R.; Scalmani, G.; Barone, V.; Mennucci, B.; Petersson, G. A.; Nakatsuji, H.; Caricato, M.; Li, X.; Hratchian, H. P.; Izmaylov, A. F.; Bloino, J.; Zheng, G.; Sonnenberg, J. L.; Hada, M.; Ehara, M.; Toyota, K.; Fukuda, R.; Hasegawa, J.; Ishida, M.; Nakajima, T.; Honda, Y.; Kitao, O.; Nakai, H.; Vreven, T.; Montgomery, J. A., Jr.; Peralta, J. E.; Ogliaro, F.; Bearpark, M.; Heyd, J. J.; Brothers, E.; Kudin, K. N.; Staroverov, V. N.; Kobayashi, R.; Normand, J.; Raghavachari, K.; Rendell, A.; Burant, J. C.; Iyengar, S. S.; Tomasi, J.; Cossi, M.; Rega, N.; Millam, J. M.; Klene, M.; Knox, J. E.; Cross, J. B.; Bakken, V.; Adamo, C.; Jaramillo, J.; Gomperts, R.; Stratmann, R. E.; Yazyev, O.; Austin, A. J.; Cammi, R.; Pomelli, C.; Ochterski, J. W.; Martin, R. L.; Morokuma, K.; Zakrzewski, V. G.; Voth, G. A.; Salvador, P.; Dannenberg, J. J.; Dapprich, S.; Daniels, A. D.; Farkas, Ö.; Foresman, J. B.; Ortiz, J. V.; Cioslowski, J.; Fox, D. J. *Gaussian 09*, revision B.01; Gaussian, Inc.: Wallingford, CT, 2009.
(27) Lever, A. B. P. *Inorganic Electronic Spectroscopy*, 2nd ed.; Elsevier Science Publishers BV: Amsterdam, The Netherlands, 1984; p 553.
(28) Buchanan, R. M.; Mashuta, M. S.; Oberhausen, K. J.; Richardson, J. F. *J. Am. Chem. Soc.* **1989**, *111*, 4497−4498.
(29) Biswas, A.; Das, L. K.; Drew, M. G. B.; Aromí, G.; Gamez, P.; Ghosh, A. *Inorg. Chem.* **2012**, *51*, 7993−8001.
(30) Marion, R.; Zaarour, M.; Qachachi, N. A.; Saleh, N. M.; Justaud, F.; Floner, D.; Lavastre, O.; Geneste, F. *J. Biol. Inorg. Chem.* **2011**, *105*, 1391−1397.
(31) Banerjee, A.; Sarkar, S.; Chopra, D.; Colacio, E.; Rajak, K. K. *Inorg. Chem.* **2008**, *47*, 4023−4031.
(32) Biswas, A.; Das, L. K.; Drew, M. G. B.; Diaz, C.; Ghosh, A. *Inorg. Chem.* **2012**, *51*, 10111−10121.
(33) Mandal, S.; Mukherjee, J.; Lloret, F.; Mukherjee, R. N. *Inorg. Chem.* **2012**, *51*, 13148−13161.
(34) Mendoza-Quijano, M. R.; Ferrer-Sueta, G.; Flores-Álamo, M.; Aliaga-Alcalde, N.; Gómez-Vidales, V.; Ugalde-Saldívara, V. M.; Gasque, L. *Dalton Trans.* **2012**, *41*, 4985−4997.
(35) Neves, A.; Rossi, L. M.; Bortoluzzi, A. J.; Szpoganicz, B.; Wiezbicki, C.; Schwingel, E. *Inorg. Chem.* **2002**, *41*, 1788−1794.
(36) Guha, A.; Chattopadhyay, T.; Paul, N. D.; Mukherjee, M.; Goswami, S.; Mondal, T. K.; Zangrando, E.; Das, D. *Inorg. Chem.* **2012**, *51*, 8750−8759.
(37) Benisvy, L.; Wanke, R.; da Silva, M. F. C. G.; Pombeiro, A. J. L. *Eur. J. Inorg. Chem.* **2011**, 2791−2796.
(38) Tyson, C. A.; Martell, A. E. *J. Am. Chem. Soc.* **1968**, *90*, 3379−3386.